Title: Electrophysiological characterisation of iPSC-derived human β-like cells and an *SLC30A8* disease model.

Running title: Coupling activity in hiPSC-derived β like cells.

Authors: Manon Jaffredo[1], Nicole A. J. Krentz[2,3], Benoite Champon[2,4], Claire E. Duff[2,4], Sameena Nawaz[4,5], Nicola Beer[4], Christian Honore[6], Anne Clark[4], Patrik Rorsman[4], Jochen Lang[1], Anna L. Gloyn[2,3,4], Matthieu Raoux[1#*], Benoit Hastoy[4,5#*] *equal contribution

Affiliations:

[1] Univ. Bordeaux, CNRS, Bordeaux INP, CBMN, UMR 5248, F-33600 Pessac, France

[2] Wellcome Centre for Human Genetics, Nuffield Department of Medicine, University of Oxford, Oxford, United Kingdom

[3] Department of Pediatrics, Stanford School of Medicine, Stanford University, CA, USA

[4] Oxford Centre for Diabetes, Endocrinology and Metabolism (OCDEM), Radcliffe Department of Medicine, University of Oxford, Oxford, United Kingdom

[5.] King Abdulaziz University and the University of Oxford Centre for Artificial Intelligence in Precision Medicine (KO-CAIPM)

[6.] Cell Therapy R&D, Novo Nordisk A/S, 2760 Måløv, Denmark.

E-mails :

Manon Jaffredo : manon.jaffredo@chu-bordeaux.fr

Nicole A. J. Krentz : nicole.krentz@ubc.ca

Benoite Champon : benoite.champon@helmholtz-muenchen.de

Claire E. Duff : claire.duff@ucl.ac.uk

Sameena Nawaz: sameena.nawaz@ocdem.ox.ac.uk

Nicola Beer: Nicola_Beer@vrtx.com

Christian Honore: clfh@novonordisk.com

Anne Clark: anne.clark@drl.ox.ac.uk

Patrik Rorsman: patrik.rorsman@ocdem.ox.ac.uk

Jochen Lang: jochen.lang@u-bordeaux.Fr

Anna L. Gloyn: agloyn@stanford.edu

Corresponding authors (#):

Matthieu Raoux (matthieu.raoux@u-bordeaux.fr)

Benoit Hastoy (benoit.hastoy@ocdem.ox.ac.uk), Tel: 0044 (0)1865857225

Keywords: hiPSC-derived Beta-like cells; *SLC30A8*; electrophysiology; Multielectrode array; electrical coupling; electrical activity, exocytosis, insulin secretion

Counts: word (4000), figures (4)

Abstract (192 words)

iPSC-derived human β-like cells (BLC) hold promise for both therapy and disease modelling, but their generation remains challenging and their functional analyses beyond transcriptomic and morphological assessments remain limited. Here, we validate an approach using multicellular and single cell electrophysiological tools to evaluate function of BLCs from pioneer protocols that can be easily adapted to more differentiated BLCs. The Multi-Electrode Arrays (MEAs) measuring the extracellular electrical activity revealed that BLCs are electrically coupled, produce slow potential (SP) signals like primary β-cells that are closely linked to insulin secretion. We also used high-resolution single-cell patch-clamp measurements to capture the exocytotic properties, and characterise voltage-gated sodium and calcium currents and found that they were comparable to those in primary β and EndoC-βH1 cells. The K_{ATP} channel conductance is greater than in human primary β-cells which may account for the limited glucose responsiveness observed with MEA. We used MEAs to study the impact of the type 2 diabetes protective *SLC30A8* allele (p.Lys34Serfs*50) and found that BLCs with this allele have stronger electrical coupling activity. Our data suggest that BLCs can be used to evaluate the functional impact of genetic variants on β-cell function and coupling.

Article highlights (75 to 100 words or fewer and should be written in complete sentences)

- iPSC-derived beta-like cells (BLCs) from pioneering protocols are widely used but needed functional electrophysiological characterizations.
- In this proof-of-concept study we used single-cell and multicellular approaches to identify signal surrogate of BLCs functions and to capture functional differences resulting from a Type 2 Diabetes (T2D)-protective *SLC30A8* allele.
- We found that BLCs shared electrophysiological features with human β-cells, and that a T2D-protective *SLC30A8* allele improves the BLCs electrical coupling activity.
- Our approach is fully applicable to more recent differentiation protocols, opens the perspective of live-monitoring the differentiation quality of BLCs, and of using them to determine the functional consequences of diabetes-associated variants.

Introduction

The differentiation of human-inducible Pluripotent Stem Cells (hiPSC) into β-like cells (BLCs) has become the favoured human cellular system to model the effects of specific alleles on β-cell development and function (1-3). However, difficulties in producing homogenous cultures of matured BLCs render functional characterisation challenging. Live recordings of extracellular electrical activity of organoids like pancreatic islets on-chip provide opportunities to address these challenges since β-cell electrical activity is tightly linked to insulin secretion (4, 5). Nutrients stimulate insulin secretion by inhibiting plasmalemmal ATP-regulated K^+ (K_{ATP}) channels leading to membrane depolarisation and action potential firing via regenerative activation of voltage-gated Na^+, Ca^{2+} and K^+ channels. The electrical activity not only regulates insulin secretion but also influences mitochondrial metabolism and gene expression (4, 6, 7). Hence, monitoring the electrical activity provides rapid and precise functional readout of BLC properties with unequalled high temporal resolution for kinetics analysis.

We used both intra- and extra-cellular electrophysiology to (i) provide a functional assessment of BLCs, and (ii) study the effect of T2D risk-associated alleles on the BLCs' function. BLCs were generated from a standard protocol of differentiation adapted from Rezania et *al.* (3) that is still widely used (8). Nevetheless, this protocol provides BLC preparations with heterogenous cellular populations that limits its overall usefulness, rendering the BLCs complex to use.

Traditional intracellular electrophysiological techniques (i.e. patch clamp) provide detailed information on specific channel activities but are low-throughput and technically demanding. Extracellular Multi-Electrode Array (MEA) recordings permit a non-invasive and easily accessible long-term monitoring of electrical activity of multicellular structures (5, 9-11). MEA captures slow potentials (SPs) (12), an electrical signal reflecting the propagation of electrical

activity across a syncytium of islet β-cells. These SPs result from the electrical coupling between β-cells and their frequency correlates with insulin secretion from human isolated pancreatic islets (5, 12). The MEA has the advantage over optical approaches in not requiring chemical probes or viral transduction of genetically encoded proteins. An additional strength is the high temporal resolution (10 kHz), much higher than that of optical techniques (typically <100Hz). Critically, MEA-recorded SPs represent a direct and unbiased coupling signal that directly correlates with insulin secretion (5).

We examined the functions of BLCs generated by the standard and most commonly used differentiation protocol (3), exploring their electrophysiological characteristics. We then applied this approach to a proof-of-concept study using BLCs expressing a T2D-protective alleles of the zinc transporter gene *SLC30A8*. Ultimately, our approach is adaptable to BLCs derived by any differentiation protocol and will facilitate the characterisation of alleles associated with or causal for diabetes on β-cell function (13-15).

Research Design and Methods

EndoC-βH1 and iPSC-derived β-like cells. Endocell provided the male EndoC-βH1 cell line. Cells were regularly tested for mycoplasma contamination (Lonza, LT07-118) and cultured as previously published (16). The female parental SB Ad3.1 hiPSC line was previously generated (17) and subjected to the following quality control checks: SNP-array testing via Human CytoSNP-12 v.2.1 beadchip (Illumina, catalog no. WG-320-2101), DAPI-stained metaphase counting and mFISH, flow cytometry for pluripotency markers (BD Biosciences, 560589 and 560126). CRISPR-Cas9 genome editing was used to generate the *SLC30A8*-p.Lys34Serfs*50 SB Ad3.1 hiPSC line and resulting cell lines were differentiated using the Rezania protocol (3) as previously described (13). At stage 4, cells were either dissociated and replated (using ROCK inhibitor to improve cell survival) onto a filter and cultured on an air-liquid interface for stage 5 to 7 to produce BLC cluster, or kept in monolayer cells and cultured in identical media composition for stage 5 to 7 to produce BLC monolayer. The first protocol is named "differentiation in cluster" and the second "differentiation in monolayer", hereafter, both protocols generating multilayers of BLCs.

Expression assays. Briefly, RNA was extracted using TRIzol Reagent (Life Technologies, 15596026) according to manufacturer's instructions. Complementary DNA was amplified using GoScript Reverse Transcription Kit (Promega, A5000). qPCR was performed using 40 ng of cDNA, TaqMan Gene Expression Master Mix (Applied Biosystems, 4369017) and primer/probes for *SLC30A8* (Hs00545182_m1), or the housekeeping gene TBP (Hs00427620_m1). Gene expression was determined using ΔΔCT method by normalising to TBP as previously published (13).

Secretion assays. iPSC-derived BLC clusters at stage 7 were incubated for 1 hr with glucose-free Krebs-Ringer buffer (KRB) medium consisting of (mM) 138 NaCl, 3.6 KCl, 0.5 $MgSO_4$,

0.5 NaH_2PO_4, 5 $NaHC0_3$, 1.5 $CaCl_2$ and 5 HEPES (adjusted to pH 7.4 with NaOH) and supplemented with 0.2% w/v BSA buffer. Depending on the quantity available, preparations were either sequentially stimulated with indicated agents or stimulated in parallel for 20 minutes. Supernatants were taken for determination of insulin release (ELISA, Alpha Laboratories) and clusters were further processed for electron microscopy.

Immunocytochemistry. BLCs were fixed in 4% paraformaldehyde, encapsulated in HistoGel (Thermo Fisher) and embedded in paraffin wax. Dewaxed 5-micron thick sections were blocked with swine serum. Insulin, glucagon and somatostatin were labelled overnight at 4°C using respectively anti-insulin (epitope: human B-chain, in house, 1/500; guinea pig), mouse anti-glucagon (Sigma, 1/500) and rabbit anti-somatostatin (Dako,1/200). The secondary antibodies (anti-guinea-pig 633, anti-mouse TRITC, and anti-rabbit 488) were diluted 1/100.

Electron microscopy. Each BLC specimen was fixed in 2.5% glutaraldehyde, and either post-fixed in 2% uranyl acetate, dehydrated in graded methanol, and embedded in London Resin Gold (Agar Scientific, Stansted, UK) or post-fixed in 1% osmium tetroxide plus 1.5% potassium ferricyanide in cacodylate buffer, and embedded in Spurr's resin. Ultrathin LRG sections (70 nm) cut onto nickel grids were immunolabelled with anti-somatostatin (Santa Cruz Biotechnology, #25262, 1:10) followed by anti-rabbit biotin (Vector Laboratories, Peterborough) and streptavidin gold 15 nm (British Biocell International, Cardiff, UK). Insulin was immunolabelled (DAKO, Ely, UK, 1:500) followed by anti-guinea pig gold 10 nm (British Biocell International). Sections were viewed on Joel 1010 microscope (accelerating voltage 80 kV) with a digital camera (Gatan, Abingdon, UK).

Intracellular electrophysiology. BLC clusters were dispersed by 3 min trypsin digestion, plated in 35 mm dishes and cultured overnight. Measurements were performed at 32°C in standard whole cell configuration using an EPC-10 amplifier and Pulse software. Exocytosis

was measured using membrane capacitance measurements. The extracellular medium contained (in mM): 118 NaCl, 5.6 KCl, 2.6 $CaCl_2$, 1.2 $MgCl_2$, 5 HEPES, and 20 tetraethylammonium (TEA) (pH 7.4 with NaOH). The intracellular medium contained (in mM): 129 CsOH, 125 Glutamic acid, 20 CsCl, 15 NaCl, 1 $MgCl_2$, 0.05 EGTA, 3 ATP, 0.1 cAMP, 5 HEPES (pH7.2 with CsOH). Cell size was estimated from the membrane capacitance. Calcium currents were measured from −40 mV to +40 mV and triggered by a 50 ms depolarisation from resting potential (−70 mV). To minimise contribution of rapidly inactivating voltage-gated sodium currents, the mean current amplitude was determined between 10-50 ms of depolarisation. Membrane potential recordings were obtained using perforated patch. The extracellular medium contained (in mM) 138 NaCl, 3.6 KCl, 0.5 $MgSO_4$, 0.5 NaH_2PO_4, 5 $NaHC0_3$, 1.5 $CaCl_2$ and 5 HEPES (pH 7.4 with NaOH). The extracellular medium was supplemented with glucose (1 or 20 mM) or tolbutamide (0.2 mM) as indicated. The intrapipette solution contained (in mM) 128 K-gluconate, 10 KCl, 10 NaCl, 1 $MgCl_2$ and 10 HEPES (pH 7.35 adjusted with KOH). Perforation of the membrane was achieved using amphotericin B (0.24 mg/ml)(6).

Extracellular electrophysiology. Recordings with MEAs were performed as published (5) at 37° C either in a solution containing (in mM): NaCl 135, KCl 4.8, $MgCl_2$ 1.2, $CaCl_2$ 2.5, HEPES 10 and glucose as indicated (pH 7.4 adjusted with NaOH) or in a more complete medium (MCDB131) without cytokines. Membranes (ALA-MEA-MEM-PL, MCS) were used to cover the MEA surface to suppress evaporation as published (12). Pictures of BLCs on MEAs were taken before and after each experiment, to localise electrodes covered with cells. Extracellular field potentials were acquired at 10 kHz per electrode, amplified and filtered (analog) at 0.1-3000 Hz with a USB-MEA60-Inv-System-E amplifier (Multichannel Systems; gain: 1200) controlled by MC_Rack software (Multichannel Systems). Data were analysed either offline or online. Offline, MC_Rack software was used to isolate SPs using a 0.2–2 Hz

band-pass digital filter (Butterworth 2nd order). For determination of frequencies, SPs were detected using the threshold module of MC_Rack with dead time (minimal period between two events) set to 300 ms. On-line hard real-time acquisition and data processing were performed with our configurable acquisition board as published (10).

Analysis and software

Data are presented as means values and SEM. Number of experiments and details of statistical analyses are in the figure legends. For electrophysiology and microscopy, n represent the number of cells from several preparation or passages of the same batch. For insulin secretion assay, n represents independent experiments from different batches of differentiation. For MEA data, n represents the number of electrodes and N the number of preparations. Sex of cells was not considered a factor in the statistical analysis. Data were analysed using R software, OriginPro 2020, and GraphPad Prism (V8.0.1).

Data and Resource Availability

The data sets generated and analysed during the current study are available from the corresponding authors upon reasonable request.

Results

Generation of hiPSC-derived BLCs. The BLCs used for the functional characterisation were obtained following the 25-day differentiation protocol adapted from Rezania *et al.* (3). (Supplementary Figure 1A). From stage 4 of the differentiation protocol, BLCs were either kept in 2D (monolayers) or replated onto filter and cultured air-liquid interface (cluster). Both monolayer and cluster protocols generate ultimately multilayers cellular structures that expressed key genes involved in β-cell maturation (*MAFA* and *PDX1)*, pancreatic hormones (*INS, GCG, SST*) and β-cell function, like K_{ATP} channel subunits (*ABCC8* and *KCNJ11*) (Supplementary Figure 1B).

We stained preparations for pancreatic hormones to ascertain the differentiation efficiency and compare them to the well-established human β-cell model, EndoC-βH1 (Supplementary Figure 1C). BLCs in monolayer produced significantly more insulin-positive cells (17.3% of 2168 BLCs cluster vs 29.7% of 471 BLCs monolayer, $p<0.001$). By contrast, all 431 EndoC-βH1 cells were insulin-positive (Supplementary Figure 1D). Glucagon-positive cells represented 10.8% and 28.2% of BLCs generated from cluster and monolayer respectively and only 1.8% of the EndoC-βH1 similarly to previous findings (6). Somatostatin was not detected in EndoC-βH1, but represented 4.9% and 7% of clusters and monolayer BLCs, respectively. These data confirm earlier observations (3) that BLCs contain polyhormonal cells: positive for glucagon or somatostatin in addition to insulin (Supplemental Figure 1C).

Closer inspection by immunogold labelling of insulin (white arrowheads) and glucagon (black arrowheads) showed distinct α-like and β-like cells with immunogold particles in vesicular structures (Supplementary Figure 1E). Some cells showed multiple types of endocrine-like vesicles: typical insulin-positive and glucagon-positive vesicles; the latter presented limited halo and two-phased electron-dense core (Supplementary Figure 1F, white arrowheads:

insulin-like vesicles, black arrowhead: glucagon-like vesicles). Insulin- and somatostatin-containing polyhormonal cells were also present with the two hormones in distinct vesicles as well as within the same vesicles (Supplementary Figure 1G, white star). Overall from the immunostaining summarised in supplementary figure 1D, we estimated that insulin positive from both BLCs presented similar proportions of co-expression with GCG and SST (Supplementary Figure 1H). We also detected typical insulin vesicles that presented an electron-dense central core surrounded by a clear halo (Supplementary Figure 1I, white arrows). Large dense core vesicles were 200 to 500 nm in diameter averaging 290 nm for monolayers and 310 nm for clusters (Supplementary Figure 1J).

Consistently with ultrastructure observations, BLCs expressed marker genes of vesicular trafficking like chromogranin A (*CHGA*), markers of the maturation of insulin like the proprotein convertase subtilisin/kexin type 1 (*PCSK1*) (Supplementary Figure 1I). Overall, the differentiation efficiency observed here is in line with previously reported outcomes for this (3) and other protocols (18-22).

Multicellular activity measured with MEAs. In islets, β-cells are electrically coupled via gap junctions and function as a syncytium (5, 9, 10, 12, 23). Electrical coupling properties can be monitored non-invasively by culturing BLCs directly on the electrodes of MEAs (Figure 1A). As human islet β-cells, the BLCs exhibited action potential (AP), seen as discrete short-lived spikes, and slow potentials (SPs) (Figure 1B). SPs are β-cell specific electrophysiological markers and result of the summation signals due to cell-cell coupling via connexin 36 (5, 12). Most BLC preparations (76.5%) were electrically active and generated both SPs and APs with similar results obtained in monolayers and in clusters (Figure 1C). However, SPs were more frequently observed in monolayers (Supplementary Figure 2A). This was consistent with the lower expression of K_{ATP} channels subunits *ABCC8* and *KCNJ11* (Supplementary figure 1B) and greater expression of connexin 36 encoded by *GJD2;* (Supplementary Figure 2B) which is

the dominant connexin expressed in human β-cells and is essential to the propagation of SP signals.

Notable differences in SPs were observed in response to β-cells activators. Our primary objective was to provide a functional quality control by the sequential addition of increasingly potent secretagogues as previously described in human islets prior to transplantation (24). In monolayers, SPs were rare at 3mM glucose and 20mM glucose alone did not increase significantly SP frequencies (Figure 1D). SP frequency significantly increased 7-fold in the presence of the adenylate cyclase activator forskolin. The effect of forskolin was more pronounced in monolayers than in clusters (Figure 1D, 1E, Supplementary Figure 3). The K_{ATP} channel blocker glibenclamide did not increase SP frequency beyond that produced by forskolin in both monolayers and clusters (Figure 1D, Supplementary Figure 3). However, a further increase was seen in the presence of the L-type Ca^{2+} channel activator Bay K8644. Inhibition of voltage-gated Ca^{2+} channels by addition of Co^{2+} (Figure 1D) or omission of extracellular Ca^{2+} (Supplementary Figure 3) abolished the SPs, in agreement with previous reports in islets (24). High glucose concentration (20 mM) only increased insulin secretion by 50% in BLC clusters (Figure 1F) echoing the weak effect on electrical activity (Figure 1D). Monitoring BLC in monolayers using an automatic real time analysis of SP frequency (9, 10) revealed that similar (50%) Glucose-Stimulated Insulin Secretion (GSIS) was associated with a dramatic but transient stimulation of the SP frequency (analysed as in (9, 10)) (Supplementary Figure 4). These differences in SP frequency are in line with *GJD2* in both BLCs models (Supplementary Figure 2).

Single-cell electrophysiological properties of BLCs. To further detail the electrophysiological properties of BLCs, we monitored their membrane potential using perforated patch whole-cell measurements. In 40% of the cells measured, increasing glucose from 1 to 20 mM induced membrane depolarisation and increased AP firing as expected from fully functional β-cell

(Figure 2A). The APs were triggered at >-40mV (Figure 2A, red inset) and their shapes and duration mirrored those reported for primary human β-cells and the human β-cell line EndoC-βH1 cells(6, 25, 26). For the remaining cells however, regenerative electrical activity (action potentials) were not present in response to glucose or tolbutamide although the cells underwent depolarisation (Figure 2B red inset). In these silent cells, the average conductance in 1 mM glucose was variable and averaged to 215.7±80.5 $pS.pF^{-1}$ (Figure 2C, top panel) corresponding to a resting potential of -66.8±0.6 mV (Figure 2C, bottom panel). This conductance is considerably larger than the conductance previously reported for human primary β-cells and EndoC-βH1 (~$60pS.pF^{-1}$) (6, 25, 26). The stimulations with either 20 mM glucose and with addition of 0.2 mM tolbutamide reduced the K_{ATP} conductance by 45% and 75% respectively promoting depolarisation of the plasma membrane (Figure 2C).

We measured the voltage-activated currents that underlie APs and trigger insulin secretion (Figure 2D). Like in primary β-cells (25), the current evoked by 50 ms depolarisation contained (i) a rapidly inactivating component (reflecting the activation of voltage-gated Na^+ channels) and (ii) a sustained component reflecting the activity of voltage-gated Ca^{2+} channels. We compared their current properties to the well-established human β-cell model EndoC-βH1(6, 16). In both cell-types, Na^+ (Figure 2E) and Ca^{2+} (Figure 2F) current densities peaked during depolarisations to 0 mV were significantly greater in BLC than in EndoC-βH1 and close to values reported in primary human β-cells(25).

Regulated exocytosis in BLCs. We first verified that BLCs expressed key components of the exocytotic machinery, such as the SNARE proteins Syntaxin1A (*STX1A*) and VAMP2 (*VAMP2*), as well as the major calcium-sensitive synaptotagmin 7 (*SYT7)* as markers of vesicular pool regulation and calcium-exocytosis coupling (27), and the calcium-insensitive synaptotagmin 4 (*SYT4)* which expression level alters insulin secretion (28) (Supplementary Figure 5A). The expressions of these genes were variable across cell-types. While *SYT7* and -

4 as well as *VAMP2* appeared to be more expressed in BLCs, the SNARE *STX1A* expression was significantly lower than in the EndoC-βH1. To further characterise the secretory capacities of BLCs, we used high-resolution membrane capacitance measurements (29, 30). This approach measures the surface area of the cells which increases in proportion to the number of vesicles inserted into the plasma membrane and releasing their content through regulated exocytosis. To estimate the kinetics of exocytosis, the cells were first subjected to depolarisations (from -70 to 0 mV) with duration ranging from 10 to 800 ms (Figure 3A). BLCs and EndoC-βH1 presented similar kinetics, reaching a maximum amplitude of exocytosis of ~10 $fF.pF^{-1}$ (Figure 3B, inset). For the shortest depolarisations (<50 ms), the amount of depolarising charges (like Ca^{2+} entry) was compared with the level of exocytosis triggered (Figure 3C). In both cell-types the amplitude of exocytosis strongly correlated with Ca^{2+} entry. However, the correlation was significantly right-shifted in BLCs. Thus, Ca^{2+} entry appears more tightly coupled to exocytosis in EndoC-βH1 cells.

We then subjected BLCs to a train of 10 depolarisations of 500 ms at 1 Hz to trigger the maximal exocytotic response (representative traces, Figure 3D). The increase in membrane capacitance per pulse was biphasic with the largest response observed during the initial 3 pulses (Figure 3E). The initial stimulation (during the first pulse) promoted significantly greater exocytotic response in BLCs than in EndoC-βH1 cells but although consistently of greater amplitude in BLCs, this difference in total exocytosis elicited did not attain statistical significance (Figure 3E, inset). Finally, the differences in current densities (Figure 2) as well as in exocytosis (Figure 3) between BLCs and EndoC-βH1 were independent of variations in cell size (Figure 3F).

A diabetes protective allele improves BLCs' electrical responses. We then used the MEA to examine the effect of a T2D-associated allele on BLCs function. As proof-of-concept, we measured the electrical behaviour of BLCs derived from a loss of function *SLC30A8* allele

(p.Lys34Serfs50*) using CRISPR-Cas9 genome-edited hiPSCs (13). Several alleles of the vesicular zinc transporter ZnT8 (*SCL30A8*) strongly influence the risk of developing T2D (13, 31). The frameshift allele p.Lys34Serfs50* provides protection against T2D and leads to loss of *SLC30A8* expression by Nonsense Mediated Decay (NMD) in homozygous BLCs (13, 31, 32). The electrical activities of BLCs generated in monolayer from the CRISPR-edited *SLC30A8* p.Lys34Serfs50* was compared to the unedited control cells (Sham) (Figure 4). In both cell lines, electrical activity was unaffected by a small increase in glucose (3 to 10 mM) (Figure 4A). Addition of forskolin or glibenclamide induced a biphasic and greater increase of SP frequency in the p.Lys34Serfs50* line but not in control BLCs (Figure 4A, B). We then subjected the preparations to 50pM GLP1 in cells exposed to 10mM glucose. SLC30A8 LOF clones presented a significant increase in SP frequency (Figure 4C-D). The expression of exocytosis markers and K_{ATP} channel subunits appeared significantly downregulated in *SLC30A8* LOF clones (Supplementary Figure 5B-C). While the consequences of the reduced *STX1A* and *SYT7* were not tested, lowered K_{ATP} channel (*ABCC8* and *KCNJ11*) expression in *SLC30A8* LOF clones likely accounts for the increased excitability measured by MEA (Figure 5). These data are in line with previous findings in EndoC-βH1 showing that *SLC30A8* knock down increased β-cells excitability through a reduced K_{ATP} channels expression (13). Finally, incubating BLCs with 10 mM glucose in complete culture medium (in presence of amino acids and additional nutrients) significantly increased SP frequency in p.Lys34Serfs50* BLCs but was without effect in the CRISPR-sham control line (Figure 4E and F). As this effect was not seen when cells were immersed in standard Krebs medium, this suggests that component of the culture medium (such as amino acids) may exert a positive effect on BLC function. This would be in line with the T2D protection associated with *SLC30A8* LOF in humans.

Discussion

Recent protocols for hiPSC-derived BLC differentiation opened new perspectives for *in vitro* human disease modelling as well as autologous diabetes cell replacement therapy (33).

While these protocols improved the functional quality of BLCs, modified pioneer protocols remain widely used (13, 34) and dynamic functional analyses are needed to better characterise and standardise these preparations (35). Our data indicate that the secretory vesicle ultrastructure and the exocytotic process in BLCs resemble those in primary human β-cells (4, 25, 29, 36). The properties of the voltage-gated Na^+ and Ca^{2+} currents in BLCs and the characteristics of APs (when generated) were likewise comparable to human primary β-cells. These data suggest that in BLCs, the exocytotic machinery required to release insulin is expressed, correctly located and functional (25, 37).

As reported previously by others using a similar protocol (3, 18-22), GSIS was clearly of small amplitude in BLCs. Several observations may explain the difference between exocytosis evoked by electrical depolarisation versus glucose-induced insulin secretion. First, K_{ATP} channel activity (expressed as membrane conductance) was considerably higher than that of mature β-cells. Although reduced upon glucose stimulation, it remained ~100 $pS.pF^{-1}$, which is sufficient to keep the cells repolarised. Second, the presence of bihormonal cells (positive for insulin and somatostatin) releasing a mixed cargo could exert a paracrine inhibitory effect through the activation of somatostatin receptor (6, 38, 39). These poly-hormonal cells, by retaining foetal properties (40, 41) and thus reducing BLC responsiveness, could contribute to a low GSIS (42, 43). Third, extracellular electrophysiology detected SPs that reflect β-cell synchronisation and strongly advocate that BLC preparations have the capability of behaving like islet micro-organs rather than the sum of isolated cells (5, 12). However, SPs frequency was low compared to primary β-cells (5, 9, 10, 12) suggesting a reduced coupling activity and reduced excitability.

The loss of function allele p.Lys34Serfs50* in *SLC30A8* leads to increased glucose responsiveness and insulin secretion in human β-cells (13). Although glucose alone did not promote an increased electrical activity, addition of forskolin alone or in presence of glibenclamide, as well as a stimulation with GLP-1 or with complete culture medium had a more potent effect on *SLC30A8* KO than on control BLCs. This is in line with recent investigation showing *SLC308* KO improved the maturation of hESC-derived β-cells (44). As coupling and SPs correlate to insulin secretion (5), our data provide an electrophysiological explanation for the enhanced insulin secretion. This is also in line with the reported reduction in K_{ATP} conductance in *SLC30A8* KD EndoC-βH1 cells and in carrier of *SLC30A8* LOF allele (13).

Our data suggest a relative immaturity of BLCs especially in the proximal (K_{ATP} channel-dependent) but not in the more distal steps of the stimulus-secretion coupling. This is in line with previous observations on low mitochondrial activities in BLCs resulting from weak TCA anaplerotic pathways (20, 45). Potentiators of glucose stimulation, like forskolin (raising cytosolic cAMP), significantly increased the SPs in BLCs, suggesting that components of incretin-dependent pathways are operational and act via stimulation of electrical activity.

Our results also suggest that functional measurements as well as gene expression should be used to follow the maturation of BLCs. Although we detected *bona fide* markers of β-cell maturation in BLCs, the better response to sulfonylureas than to glucose echoes foetal β-cells properties (46). This reignites the debate as to whether markers like *MAFA* levels represent a good marker of human BLC maturity (47) and highlights the challenge of predicting β-cell function and maturity from transcriptomic data. Clearly, the best measure of BLC maturity remains the response to physiological concentrations of glucose and other secretagogues capturing the sequence of molecular mechanisms reported in human pancreatic islets (membrane depolarisation, coupling, stimulation of insulin secretion).

In conclusion, our data illustrate that functional assessment of BLCs requires a multifaceted approach combining measurements from bulk, micro-organ and single-cells. We provide here a proof-of-concept study that paves the way for functional investigations in BLCs generated from more recent protocol of differentiation and offers the possibility to be integrated in a quality control or drug-screening pipeline. The electrophysiological characterisation of BLCs, as done here, provides a starting point to understanding functional characteristics of the different maturation stages of BLCs and highlights its usefulness to investigate cellular consequences of specific alleles in human β-cells.

Acknowledgements:

Contribution: M.J., N.A.J.K, C.E.D., N.B., C.H., A.C, B.C., S.N., M.R., B.H.: collected the data. P.R., J.L., A.L.G., A.C, N.B., C.H., C.E.D., N.A.J.K.: edited the manuscript; M.R, B.H: *equal contribution, designed the study, analysed data and wrote the manuscript.

Conflicts of Interest: ALG's spouse is an employee of Genentech and holds stock options in Roche. NLB was an employee of University of Oxford when all work contained in this manuscript was conducted. CH is an employee and stock holder of Novo Nordisk A/S. No other potential conflicts of interest relevant to this article were reported.

Funding: BH is a Diabetes UK R.D. Lawrence Fellow (BDA number:19/0005965) and is also supported by King Abdulaziz University & Oxford University Centre for Artificial Intelligence in Precision Medicines (KO-CAIPM). M.J. is supported by an EFSD Albert Renold award, MJ & MR are supported by the French Ministry of Research & Education, JL is supported by the FEDER DIAGLYC & ANR DIABLO (ANR-18-CE17-0005). ALG is a Wellcome Trust Senior Fellow in Basic Biomedical Science. Work in ALG's laboratory was funded by the Wellcome Trust (200837), and the National Institutes of Health (UM-1DK126185). M.R. & B.H. are the guarantors of this study.

References (<50ref)

1. Aguayo-Mazzucato C, Bonner-Weir S. Pancreatic beta Cell Regeneration as a Possible Therapy for Diabetes. Cell Metab. 2018;27(1):57-67.
2. Pagliuca FW, Millman JR, Gurtler M, Segel M, Van Dervort A, Ryu JH, et al. Generation of functional human pancreatic beta cells in vitro. Cell. 2014;159(2):428-39.
3. Rezania A, Bruin JE, Arora P, Rubin A, Batushansky I, Asadi A, et al. Reversal of diabetes with insulin-producing cells derived in vitro from human pluripotent stem cells. Nat Biotechnol. 2014;32(11):1121-33.
4. Rorsman P, Ashcroft FM. Pancreatic beta-Cell Electrical Activity and Insulin Secretion: Of Mice and Men. Physiol Rev. 2018;98(1):117-214.
5. Jaffredo M, Bertin E, Pirog A, Puginier E, Gaitan J, Oucherif S, et al. Dynamic Uni- and Multicellular Patterns Encode Biphasic Activity in Pancreatic Islets. Diabetes. 2021;70(4):878-88.
6. Hastoy B, Godazgar M, Clark A, Nylander V, Spiliotis I, van de Bunt M, et al. Electrophysiological properties of human beta-cell lines EndoC-betaH1 and -betaH2 conform with human beta-cells. Sci Rep. 2018;8(1):16994.
7. Sabatini PV, Speckmann T, Lynn FC. Friend and foe: beta-cell Ca(2+) signaling and the development of diabetes. Mol Metab. 2019;21:1-12.
8. Lau HH, Krentz NAJ, Abaitua F, Perez-Alcantara M, Chan JW, Ajeian J, et al. PAX4 loss of function increases diabetes risk by altering human pancreatic endocrine cell development. Nat Commun. 2023;14(1):6119.
9. Pedraza E, Karajic A, Raoux M, Perrier R, Pirog A, Lebreton F, et al. Guiding pancreatic beta cells to target electrodes in a whole-cell biosensor for diabetes. Lab Chip. 2015;15(19):3880-90.
10. Perrier R, Pirog A, Jaffredo M, Gaitan J, Catargi B, Renaud S, et al. Bioelectronic organ-based sensor for microfluidic real-time analysis of the demand in insulin. Biosens Bioelectron. 2018;117:253-9.
11. Raoux M, Bornat Y, Quotb A, Catargi B, Renaud S, Lang J. Non-invasive long-term and real-time analysis of endocrine cells on micro-electrode arrays. J Physiol. 2012;590(5):1085-91.

12. Lebreton F, Pirog A, Belouah I, Bosco D, Berney T, Meda P, et al. Slow potentials encode intercellular coupling and insulin demand in pancreatic beta cells. Diabetologia. 2015;58(6):1291-9.
13. Dwivedi OP, Lehtovirta M, Hastoy B, Chandra V, Krentz NAJ, Kleiner S, et al. Loss of ZnT8 function protects against diabetes by enhanced insulin secretion. Nat Genet. 2019;51(11):1596-606.
14. Lytrivi M, Senee V, Salpea P, Fantuzzi F, Philippi A, Abdulkarim B, et al. DNAJC3 deficiency induces beta-cell mitochondrial apoptosis and causes syndromic young-onset diabetes. Eur J Endocrinol. 2021;184(3):455-68.
15. Perez-Alcantara M, Honore C, Wesolowska-Andersen A, Gloyn AL, McCarthy MI, Hansson M, et al. Patterns of differential gene expression in a cellular model of human islet development, and relationship to type 2 diabetes predisposition. Diabetologia. 2018;61(7):1614-22.
16. Ravassard P, Hazhouz Y, Pechberty S, Bricout-Neveu E, Armanet M, Czernichow P, et al. A genetically engineered human pancreatic beta cell line exhibiting glucose-inducible insulin secretion. J Clin Invest. 2011;121(9):3589-97.
17. van de Bunt M, Lako M, Barrett A, Gloyn AL, Hansson M, McCarthy MI, et al. Insights into islet development and biology through characterization of a human iPSC-derived endocrine pancreas model. Islets. 2016;8(3):83-95.
18. Balboa D, Saarimaki-Vire J, Borshagovski D, Survila M, Lindholm P, Galli E, et al. Insulin mutations impair beta-cell development in a patient-derived iPSC model of neonatal diabetes. Elife. 2018;7.
19. Lithovius V, Saarimaki-Vire J, Balboa D, Ibrahim H, Montaser H, Barsby T, et al. SUR1-mutant iPS cell-derived islets recapitulate the pathophysiology of congenital hyperinsulinism. Diabetologia. 2021;64(3):630-40.
20. Davis JC, Alves TC, Helman A, Chen JC, Kenty JH, Cardone RL, et al. Glucose Response by Stem Cell-Derived beta Cells In Vitro Is Inhibited by a Bottleneck in Glycolysis. Cell Rep. 2020;31(6):107623.
21. Russ HA, Parent AV, Ringler JJ, Hennings TG, Nair GG, Shveygert M, et al. Controlled induction of human pancreatic progenitors produces functional beta-like cells in vitro. EMBO J. 2015;34(13):1759-72.
22. Zhu S, Russ HA, Wang X, Zhang M, Ma T, Xu T, et al. Human pancreatic beta-like cells converted from fibroblasts. Nat Commun. 2016;7:10080.

23. Bavamian S, Klee P, Britan A, Populaire C, Caille D, Cancela J, et al. Islet-cell-to-cell communication as basis for normal insulin secretion. Diabetes Obes Metab. 2007;9 Suppl 2:118-32.
24. Raoux M, Lablanche S, Jaffredo M, Pirog A, Benhamou PY, Lebreton F, et al. Islets-on-Chip: A Tool for Real-Time Assessment of Islet Function Prior to Transplantation. Transpl Int. 2023;36:11512.
25. Braun M, Ramracheya R, Bengtsson M, Zhang Q, Karanauskaite J, Partridge C, et al. Voltage-gated ion channels in human pancreatic beta-cells: electrophysiological characterization and role in insulin secretion. Diabetes. 2008;57(6):1618-28.
26. Rorsman P, Braun M. Regulation of insulin secretion in human pancreatic islets. Annu Rev Physiol. 2013;75:155-79.
27. Dolai S, Xie L, Zhu D, Liang T, Qin T, Xie H, et al. Synaptotagmin-7 Functions to Replenish Insulin Granules for Exocytosis in Human Islet beta-Cells. Diabetes. 2016;65(7):1962-76.
28. Huang C, Walker EM, Dadi PK, Hu R, Xu Y, Zhang W, et al. Synaptotagmin 4 Regulates Pancreatic beta Cell Maturation by Modulating the Ca(2+) Sensitivity of Insulin Secretion Vesicles. Dev Cell. 2018;45(3):347-61 e5.
29. Gillis KD, Misler S. Single cell assay of exocytosis from pancreatic islet B cells. Pflugers Arch. 1992;420(1):121-3.
30. Katz B, Miledi R. A study of synaptic transmission in the absence of nerve impulses. J Physiol. 1967;192(2):407-36.
31. Flannick J, Thorleifsson G, Beer NL, Jacobs SB, Grarup N, Burtt NP, et al. Loss-of-function mutations in SLC30A8 protect against type 2 diabetes. Nat Genet. 2014;46(4):357-63.
32. Krentz NAJ, Gloyn AL. Insights into pancreatic islet cell dysfunction from type 2 diabetes mellitus genetics. Nat Rev Endocrinol. 2020;16(4):202-12.
33. Maxwell KG, Millman JR. Applications of iPSC-derived beta cells from patients with diabetes. Cell Rep Med. 2021;2(4):100238.
34. Mattis KK, Gloyn AL. From Genetic Association to Molecular Mechanisms for Islet-cell Dysfunction in Type 2 Diabetes. J Mol Biol. 2020;432(5):1551-78.
35. Bourgeois S, Sawatani T, Van Mulders A, De Leu N, Heremans Y, Heimberg H, et al. Towards a Functional Cure for Diabetes Using Stem Cell-Derived Beta Cells: Are We There Yet? Cells. 2021;10(1).

36. Braun M, Ramracheya R, Johnson PR, Rorsman P. Exocytotic properties of human pancreatic beta-cells. Ann N Y Acad Sci. 2009;1152:187-93.
37. Hastoy B, Clark A, Rorsman P, Lang J. Fusion pore in exocytosis: More than an exit gate? A beta-cell perspective. Cell Calcium. 2017;68:45-61.
38. Hauge-Evans AC, King AJ, Carmignac D, Richardson CC, Robinson IC, Low MJ, et al. Somatostatin secreted by islet delta-cells fulfills multiple roles as a paracrine regulator of islet function. Diabetes. 2009;58(2):403-11.
39. Strowski MZ, Parmar RM, Blake AD, Schaeffer JM. Somatostatin inhibits insulin and glucagon secretion via two receptors subtypes: an in vitro study of pancreatic islets from somatostatin receptor 2 knockout mice. Endocrinology. 2000;141(1):111-7.
40. Jennings RE, Berry AA, Kirkwood-Wilson R, Roberts NA, Hearn T, Salisbury RJ, et al. Development of the human pancreas from foregut to endocrine commitment. Diabetes. 2013;62(10):3514-22.
41. Riedel MJ, Asadi A, Wang R, Ao Z, Warnock GL, Kieffer TJ. Immunohistochemical characterisation of cells co-producing insulin and glucagon in the developing human pancreas. Diabetologia. 2012;55(2):372-81.
42. Henquin JC, Nenquin M. Immaturity of insulin secretion by pancreatic islets isolated from one human neonate. J Diabetes Investig. 2018;9(2):270-3.
43. Helman A, Cangelosi AL, Davis JC, Pham Q, Rothman A, Faust AL, et al. A Nutrient-Sensing Transition at Birth Triggers Glucose-Responsive Insulin Secretion. Cell Metab. 2020;31(5):1004-16 e5.
44. Ma Q, Xiao Y, Xu W, Wang M, Li S, Yang Z, et al. ZnT8 loss-of-function accelerates functional maturation of hESC-derived beta cells and resists metabolic stress in diabetes. Nat Commun. 2022;13(1):4142.
45. Balboa D, Barsby T, Lithovius V, Saarimaki-Vire J, Omar-Hmeadi M, Dyachok O, et al. Functional, metabolic and transcriptional maturation of human pancreatic islets derived from stem cells. Nat Biotechnol. 2022;40(7):1042-55.
46. Rorsman P, Arkhammar P, Bokvist K, Hellerstrom C, Nilsson T, Welsh M, et al. Failure of glucose to elicit a normal secretory response in fetal pancreatic beta cells results from glucose insensitivity of the ATP-regulated K+ channels. Proc Natl Acad Sci U S A. 1989;86(12):4505-9.
47. Jacobson EF, Tzanakakis ES. Human pluripotent stem cell differentiation to functional pancreatic cells for diabetes therapies: Innovations, challenges and future directions. J Biol Eng. 2017;11:21.

Figures legends

Figure 1: Multicellular MEA analysis of BLCs reveals electrical coupling. A. Picture of a MEA (top, scale bar: 1 cm) with BLCs (in clusters) cultured on the 59 electrodes (bottom, scale bar: 200 µm). **B**. Representative recordings of the electrical activity of primary human islet β cells (top) and BLCs (bottom) obtained from one of the MEA-electrodes. The two characteristic types of electrical signals were present in both cells: the multicellular SPs (examples in red) and the unicellular APs (examples in blue). See also Supplementary Fig. 2 for comparison with recordings of EndoC-βH1 cells. **C.** Inter-preparation analysis. Proportion BLC preparations presenting SPs and APs (black), only APs (grey) or neither SPs nor APs (white). Data for all preparations (All: clusters and monolayers), monolayers only (Mono) and clusters only are presented. **D.** MEA-based functional quality control of a preparation of BLCs in monolayer (Mono). Variations of SP frequencies (top: means values ±SEM; bottom: statistics performed on areas under the curves (AUC) normalised over time; last 5 min for G3 and first 5 min for the other conditions) in response to several stimuli: 3 mM glucose (G3), 20 mM glucose (G20) alone, followed by successive additions of forskolin (Fsk, 1 µM), glibenclamide (Glib, 100 nM) and Bay K8644 (Bay, 10 µM). At the end of the protocol, G3 with $CoCl_2$ (Co, 2 mM) was applied to inhibit the electrical activity. (n=27; **p<0.01, *** p<0.001, **** p<0.0001; Friedman test). See also Supplementary Fig. 3 for the same quality control on a preparation of BLCs in clusters. **E.** Electrical responses to high glucose and Fsk (HG/Fsk) were represented as fold change of AUC SP frequency relative to low glucose (LG), and were higher in monolayers than in clusters (Mono, N=4; Clusters, N=2; Welch's t-test). **F.** Glucose stimulation (20mM) in clusters preparations elicited a mild but significant increase in insulin secretion (N=5, 2p=0.025, two-tail ratio paired t-test).

Figure 2: Single-cell electrical properties of BLCs. A. BLC membrane potential recording in an active cell upon incubation with 1 and 20mM glucose and representative action potential

(red inset). **B.** Representative recording of a silent cell. Increase glucose concentration promoted slight membrane depolarisation but did not translate in AP firing (red inset) **C.** Relationship between K_{ATP} channel conductance (top panel) and membrane potential (bottom panel) from silent BLCs at 1mM, 20 mM glucose and with 0.2 mM tolbutamide. (n=3 cells) **D**. Representative trace of current elicited by a square depolarisation from the resting potential (-70 mV) to 0 mV. The inward current is composed of a rapid (<5 ms) sodium component (thin black section) followed by a sustained calcium component (black section in bold). **E-F.** Current-voltage relationship for the sodium (E) and calcium (F) components. Black: EndoC-βH1 (n=10 cells) and BLC in red (n=17 cells).* p<0.05, ** p<0.01, *** p<0.001 Paired comparison and Tukey.

Figure 3: Comparison of the exocytotic properties of BLCs and EndoC-βH1 cells. A-B. EndoC-βH1 (black) and BLCs dispersed from cluster preparations (red) were subjected to increased durations of depolarisation (from 10 ms to 800 ms) and the resulting exocytosis events were measured as an increase in cell surface area. **B.** The stimulations triggered similar kinetics of exocytosis in both models with a plateau reached from 300ms depolarisation. Inset: maximum exocytosis elicited by 800ms stimulation (n=13 and n=15 cells for EndoC-βh1, black, and BLC, red, respectively). **C.** Charge-exocytosis relationship in EndoC-βH1 and in BLC. The right-shifted correlation in BLCs is driven significantly by the amount charges. **D.** Representative traces of the maximum exocytosis elicited by ten depolarisations of 500 ms. **E.** Quantification of exocytosis increment elicited at each pulse (n=13 and 11 cells for EndoC-βH1 and BLC, respectively). Insert: total cumulative exocytosis measured at pulse 10. **F.** The initial size of the cells (pF) were similar between the two β-cell models (n=13 and n=15 cells for EndoC-βh1, black, and BLC, red, respectively). Statistics, **p<0.01, *** p<0.001, Paired comparison and Bonferroni posthoc test.

Figure 4: The loss-of-function mutation of *SLC30A8* increases slow potential frequencies in CRISPR-edited BLC monolayers.

A. Kinetics of average SP frequencies measured in CRISPR-Sham (black) and *SLC30A8*-edited BLCs (red) in the presence of 3 mM (G3), and 10 mM (G10) glucose alone followed by successive additions of forskolin (Fsk, 1 μM) and glibenclamide (Glib, 100 nM, in the presence of Fsk). **B**. Statistics on AUCs of SP frequencies (normalised over time; last 5 min for G3 and first 5 min for the other conditions) obtained from data in (A) (n=23-40; N=2 independent mutated clones; *p<0.05, *** p<0.001, **** p<0.0001; Kruskal-Wallis test). **C.** The loss-of-function variant of *SLC30A8* increases electrical responses to physiological levels of the intestinal incretin hormone GLP-1 in CRISPR-edited BLCs. Kinetics of SP frequency in CRISPR-Sham (black) and *SLC30A8*-edited (red) monolayer BLCs when 50 pM GLP-1 is applied in the continuous presence 10 mM (G10) glucose. **D.** Statistics on AUCs of SP frequencies upon GLP-1 (first 5 min) obtained from data in (C) (n=12-26; *** p<0.001; Mann Whitney test). **E**. SP frequencies measured on the same BLCs at 10 mM glucose in the presence of a standard saline solution and in of complete medium. **F**. Statistics on AUCs of SP frequencies (normalised over time) of data in C (n=23-40; N=2; **** p<0.0001; Kruskal-Wallis test).

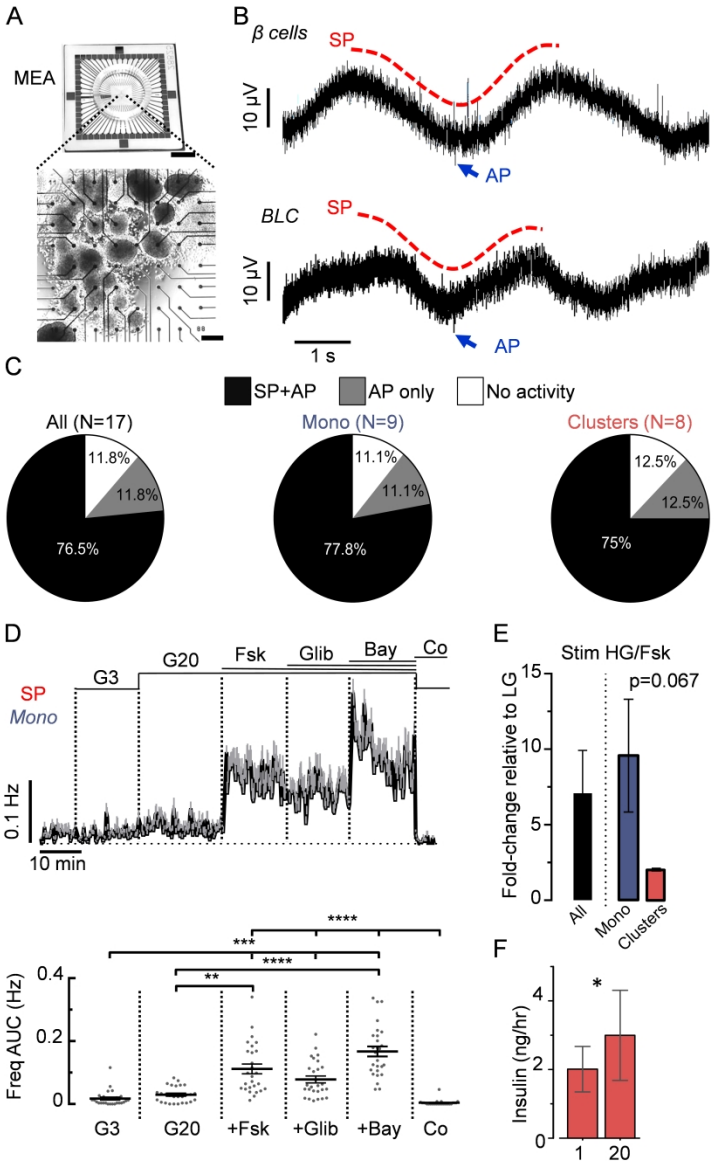

Figure 1: Multicellular MEA analysis of BLCs reveals electrical coupling. A. Picture of a MEA (top, scale bar: 1 cm) with BLCs (in clusters) cultured on the 59 electrodes (bottom, scale bar: 200 µm). B. Representative recordings of the electrical activity of primary human islet β cells (top) and BLCs (bottom) obtained from one of the MEA-electrodes. The two characteristic types of electrical signals were present in both cells: the multicellular SPs (examples in red) and the unicellular APs (examples in blue). See also Supplementary Fig. 2 for comparison with recordings of EndoC-βH1 cells. C. Inter-preparation analysis. Proportion BLC preparations presenting SPs and APs (black), only APs (grey) or neither SPs nor APs (white). Data for all preparations (All: clusters and monolayers), monolayers only (Mono) and clusters only are presented. D. MEA-based functional quality control of a preparation of BLCs in monolayer (Mono). Variations of SP frequencies (top: means values +SEM; bottom: statistics performed on areas under the curves (AUC) normalised over time; last 5 min for G3 and first 5 min for the other conditions) in response to several stimuli: 3 mM glucose (G3), 20 mM glucose (G20) alone, followed by successive additions of forskolin (Fsk, 1 µM), glibenclamide (Glib, 100 nM) and Bay K8644 (Bay, 10 µM). At the end of the protocol, G3 with CoCl2 (Co, 2 mM) was applied to inhibit the electrical activity. (n=27; **p<0.01, *** p<0.001, **** p<0.0001;

Friedman test). See also Supplementary Fig. 3 for the same quality control on a preparation of BLCs in clusters. E. Electrical responses to high glucose and Fsk (HG/Fsk) were represented as fold change of AUC SP frequency relative to low glucose (LG), and were higher in monolayers than in clusters (Mono, N=4; Clusters, N=2; Welch's t-test). F. Glucose stimulation (20mM) in clusters preparations elicited a mild but significant increase in insulin secretion (N=5, 2p=0.025, two-tail ratio paired t-test).

1187x1919mm (96 x 96 DPI)

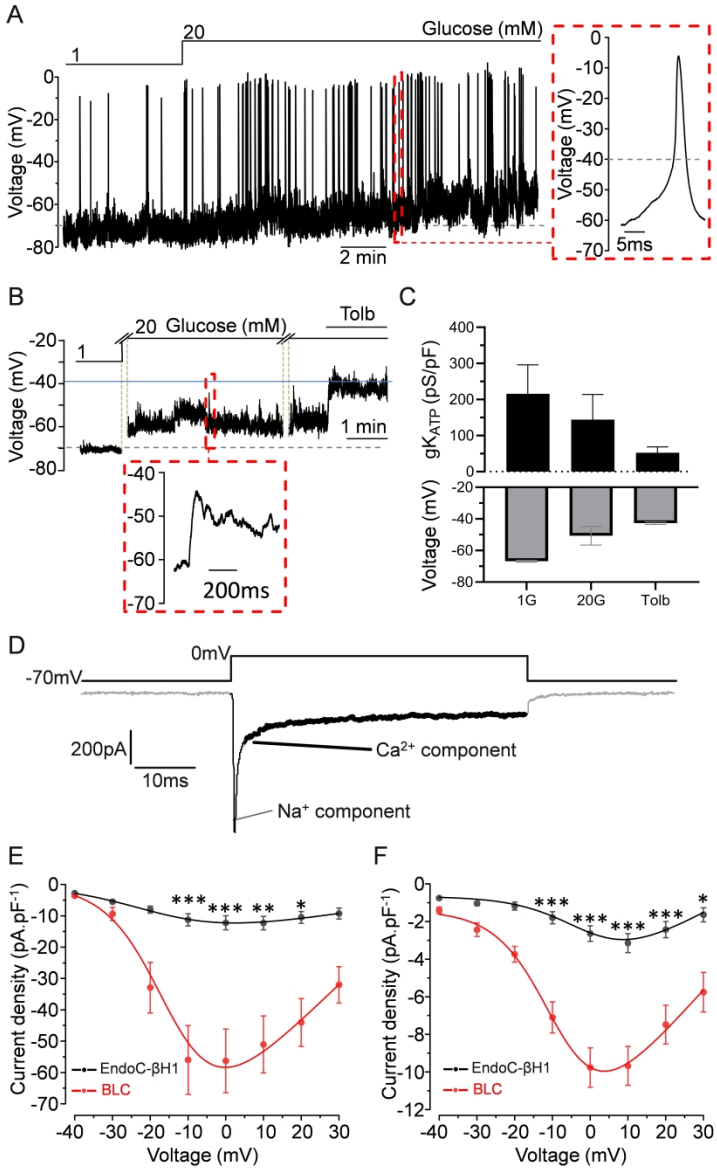

Figure 2: Single-cell electrical properties of BLCs. A. BLC membrane potential recording in an active cell upon incubation with 1 and 20mM glucose and representative action potential (red inset). B. Representative recording of a silent cell. Increase glucose concentration promoted slight membrane depolarisation but did not translate in AP firing (red inset) C. Relationship between KATP channel conductance (top panel) and membrane potential (bottom panel) from silent BLCs at 1mM, 20 mM glucose and with 0.2 mM tolbutamide. (n=3 cells) D. Representative trace of current elicited by a square depolarisation from the resting potential (-70 mV) to 0 mV. The inward current is composed of a rapid (<5 ms) sodium component (thin black section) followed by a sustained calcium component (black section in bold). E-F. Current-voltage relationship for the sodium (E) and calcium (F) components. Black: EndoC-βH1 (n=10 cells) and BLC in red (n=17 cells).* p<0.05, ** p<0.01, *** p<0.001 Paired comparison and Tukey.

1187x1919mm (96 x 96 DPI)

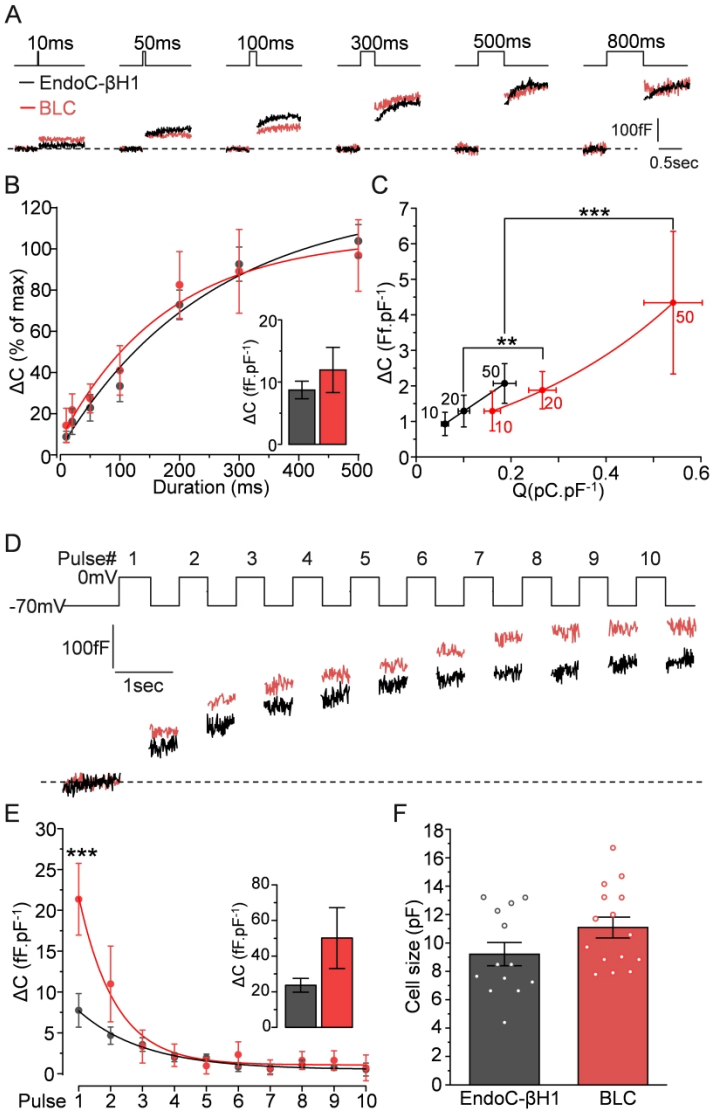

Figure 3: Comparison of the exocytotic properties of BLCs and EndoC-βH1 cells. A-B. EndoC-βH1 (black) and BLCs dispersed from cluster preparations (red) were subjected to increased durations of depolarisation (from 10 ms to 800 ms) and the resulting exocytosis events were measured as an increase in cell surface area. B. The stimulations triggered similar kinetics of exocytosis in both models with a plateau reached from 300ms depolarisation. Inset: maximum exocytosis elicited by 800ms stimulation (n=13 and n=15 cells for EndoC-βh1, black, and BLC, red, respectively). C. Charge-exocytosis relationship in EndoC-βH1 and in BLC. The right-shifted correlation in BLCs is driven significantly by the amount charges. D. Representative traces of the maximum exocytosis elicited by ten depolarisations of 500 ms. E. Quantification of exocytosis increment elicited at each pulse (n=13 and 11 cells for EndoC-βH1 and BLC, respectively). Insert: total cumulative exocytosis measured at pulse 10. F. The initial size of the cells (pF) were similar between the two β-cell models (n=13 and n=15 cells for EndoC-βh1, black, and BLC, red, respectively). Statistics, **p<0.01, *** p<0.001, Paired comparison and Bonferroni posthoc test.

1187x1919mm (96 x 96 DPI)

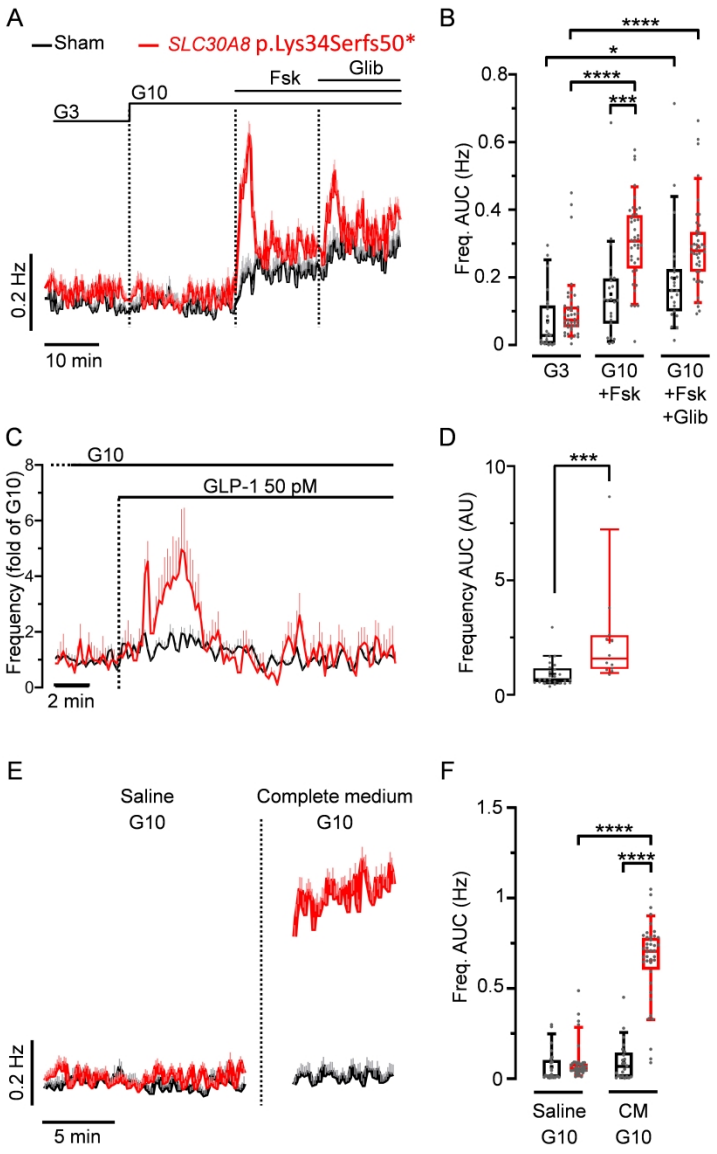

Figure 4: The loss-of-function mutation of SLC30A8 increases slow potential frequencies in CRISPR-edited BLC monolayers. A. Kinetics of average SP frequencies measured in CRISPR-Sham (black) and SLC30A8-edited BLCs (red) in the presence of 3 mM (G3), and 10 mM (G10) glucose alone followed by successive additions of forskolin (Fsk, 1 µM) and glibenclamide (Glib, 100 nM, in the presence of Fsk). B. Statistics on AUCs of SP frequencies (normalised over time; last 5 min for G3 and first 5 min for the other conditions) obtained from data in (A) (n=23-40; N=2 independent mutated clones; *p<0.05, *** p<0.001, **** p<0.0001; Kruskal-Wallis test). C. The loss-of-function variant of SLC30A8 increases electrical responses to physiological levels of the intestinal incretin hormone GLP-1 in CRISPR-edited BLCs. Kinetics of SP frequency in CRISPR-Sham (black) and SLC30A8-edited (red) monolayer BLCs when 50 pM GLP-1 is applied in the continuous presence 10 mM (G10) glucose. D. Statistics on AUCs of SP frequencies upon GLP-1 (first 5 min) obtained from data in (C) (n=12-26; *** p<0.001; Mann Whitney test). E. SP frequencies measured on the same BLCs at 10 mM glucose in the presence of a standard saline solution and in of complete medium. F. Statistics on AUCs of SP frequencies (normalised over time) of data in C (n=23-40; N=2; **** p<0.0001; Kruskal-Wallis test).

1187x1919mm (96 x 96 DPI)

Supplementary Material

Electrophysiological characterisation of iPSC-derived human β-like cells and an *SLC30A8* disease model.

Manon Jaffredo[1], Nicole A. J. Krentz[2,3], Benoite Champon[2,4], Claire E. Duff[2,4], Sameena Nawaz[4], Nicola Beer[4], Christian Honore[5], Anne Clark[4], Patrik Rorsman[4], Jochen Lang[1], Anna L. Gloyn[2,3,4], Matthieu Raoux[1#], Benoit Hastoy[4#]

[1] Univ. Bordeaux, CNRS, Bordeaux INP, CBMN, UMR 5248, F-33600 Pessac, France

[2] Wellcome Centre for Human Genetics, Nuffield Department of Medicine, University of Oxford, Oxford, United Kingdom

[3] Department of Pediatrics, Stanford School of Medicine, Stanford University, CA, USA

[4] Oxford Centre for Diabetes, Endocrinology and Metabolism (OCDEM), Radcliffe Department of Medicine, University of Oxford, Oxford, United Kingdom

[5] Cell Therapy R&D, Novo Nordisk A/S, 2760 Måløv, Denmark.

Corresponding authors:

Matthieu Raoux (matthieu.raoux@u-bordeaux.fr)

Benoit Hastoy (benoit.hastoy@ocdem.ox.ac.uk)

Supplementary figures:

Supplementary Figure 1: Overview of the characterisation of iPSC derived BLCs.

Supplementary Figure 2: Intra-preparation analysis of SPs with MEAs and *GJD2* expression in monolayer vs. clusters.

Supplementary Figure 3: Functional quality control with MEAs of a cluster preparation of BLCs.

Supplementary Figure 4: Combination of automatic microelectronic analysis of SPs and insulin secretion.

Supplementary Figure 5: Gene expression of key markers of secretory function in BLCs cluster and monolayer and in *SLC30A8*-edited clones.

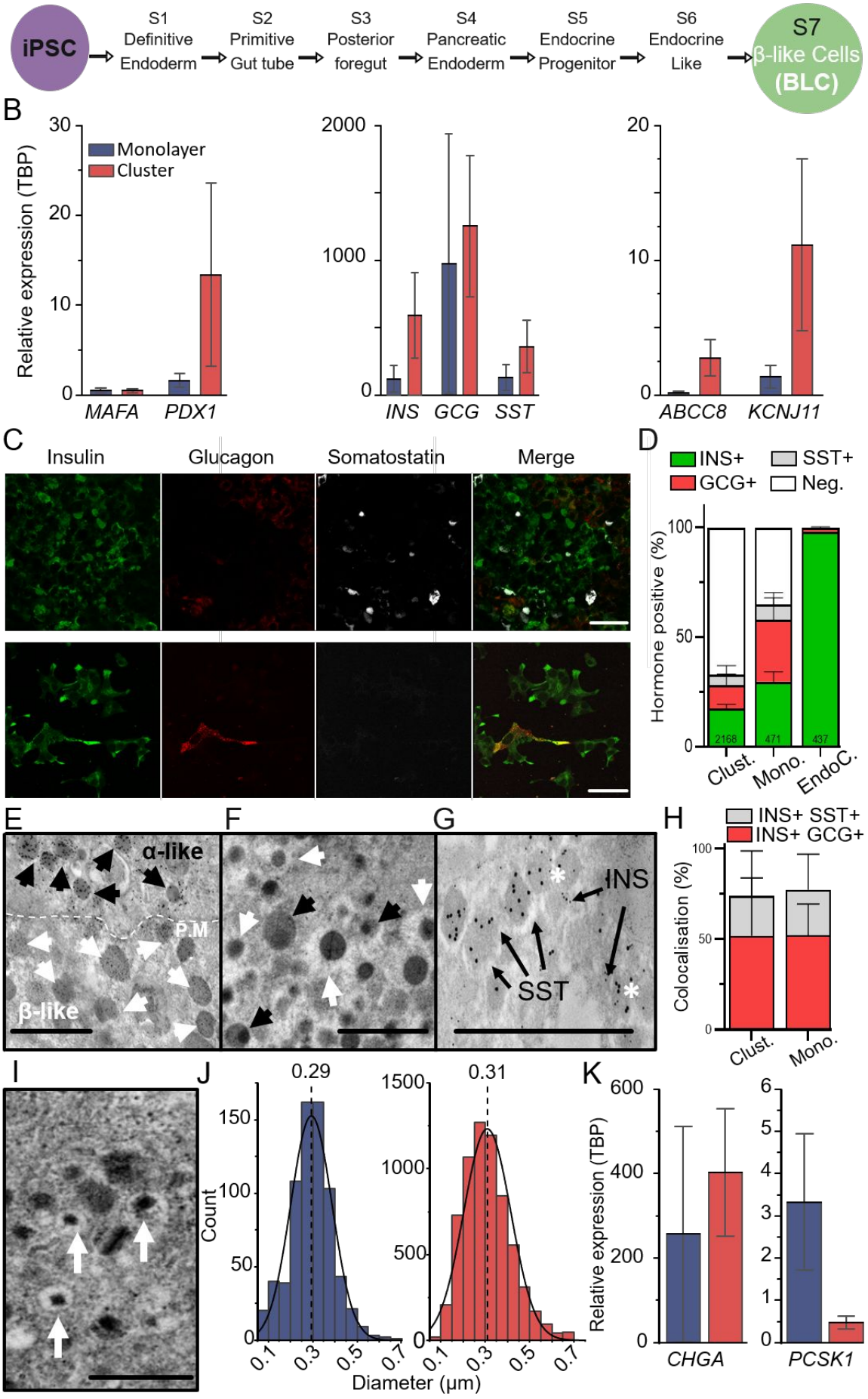

Supplementary Figure 1: Overview of the characterisation of iPSC derived BLCs. A. iPSC were derived following the 25-day differentiation protocol. **B.** RT-qPCR data shows variability in the expressions of differentiation markers (left, n_{cl}=8, n_{mono}=4), pancreatic hormones (centre, n_{cl}=8, n_{mono}=4-5), and K_{ATP} channels subunits (right, n_{cl}=9, n_{mono}=4). **C.** Immunostaining against pancreatic hormones in BLC (cluster) and EndoC-βH1. Preparations were stained for Insulin (green), Glucagon (red), and somatostatin (white). Scale bar 50µm. **D.** Proportion of insulin-, glucagon- and somatostatin-positive cells among 2168 cluster BLCs (Clust.), 471 monolayer BLCs (Mono.), and 431 EndoC-βH1 cells (EndoC.). **E-G**, ultrastructure of BLCs. **E.** Immunogold labelling of cells expressing either insulin (10nm gold particles, white arrowhead, BLC) or either glucagon (15nm gold particles, black arrowheads, α-like cell). PM, Plasma Membrane (dash line). **F.** Electron micrograph of a polyhormonal cell presenting heterogeneous vesicular structures, some typical of glucagon containing vesicles (black arrow heads) or of insulin containing vesicles (white arrowheads). **G.** Immunogold labelling of a polyhormonal cell positive for insulin (10nm gold particles) and somatostatin (SST, 15nm). The hormones could be detected in independent and within the same vesicles (white stars). Scale bar 1µm. **H.** Proportion of polyhormonal cells BLCs positive for insulin and with either somatostatin (grey) or glucagon (red) generated from cluster (Clust.) and monolayers (Mono.). **I.** Representative electron micrographs of cells containing structurally matured insulin vesicles (white arrows). Scale bar 0.5µm **J.** Vesicle size distribution in clusters and monolayers (n_{mono}=713 and n_{cl}=6532 vesicles). **K.** BLCs express components of the trafficking pathway *CHGA* (left), component of insulin maturation *PCSK1*(right) (n_{cl}=6, n_{mono}=3).

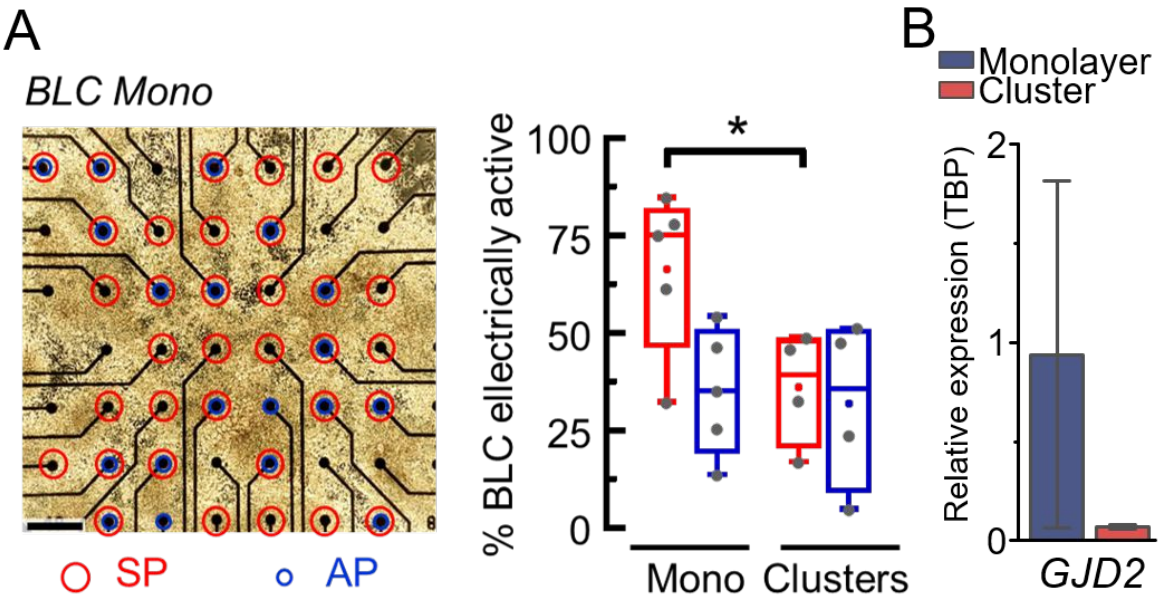

Supplementary Figure 2

Supplementary Figure 2: Intra-preparation analysis of SPs with MEAs and *GJD2* expression in monolayer vs. clusters. (**A**) Intra-preparation analysis. Left: monolayer of BLCs on a MEA. The electrodes that detected SPs are circled in red and those detecting APs are circled blue. For each experiment, some electrodes could record both or one or none of these electrical. Right: proportion of electrodes with SPs (red) or APs (blue) for each preparation (All, N=9 MEAs; Mono, N=5 MEAs; Clusters, N=4 MEAs; *p<0.05; t-test). (**B**) BLCs express cellular coupling marker *GJD2* essential in the propagation of SPs.

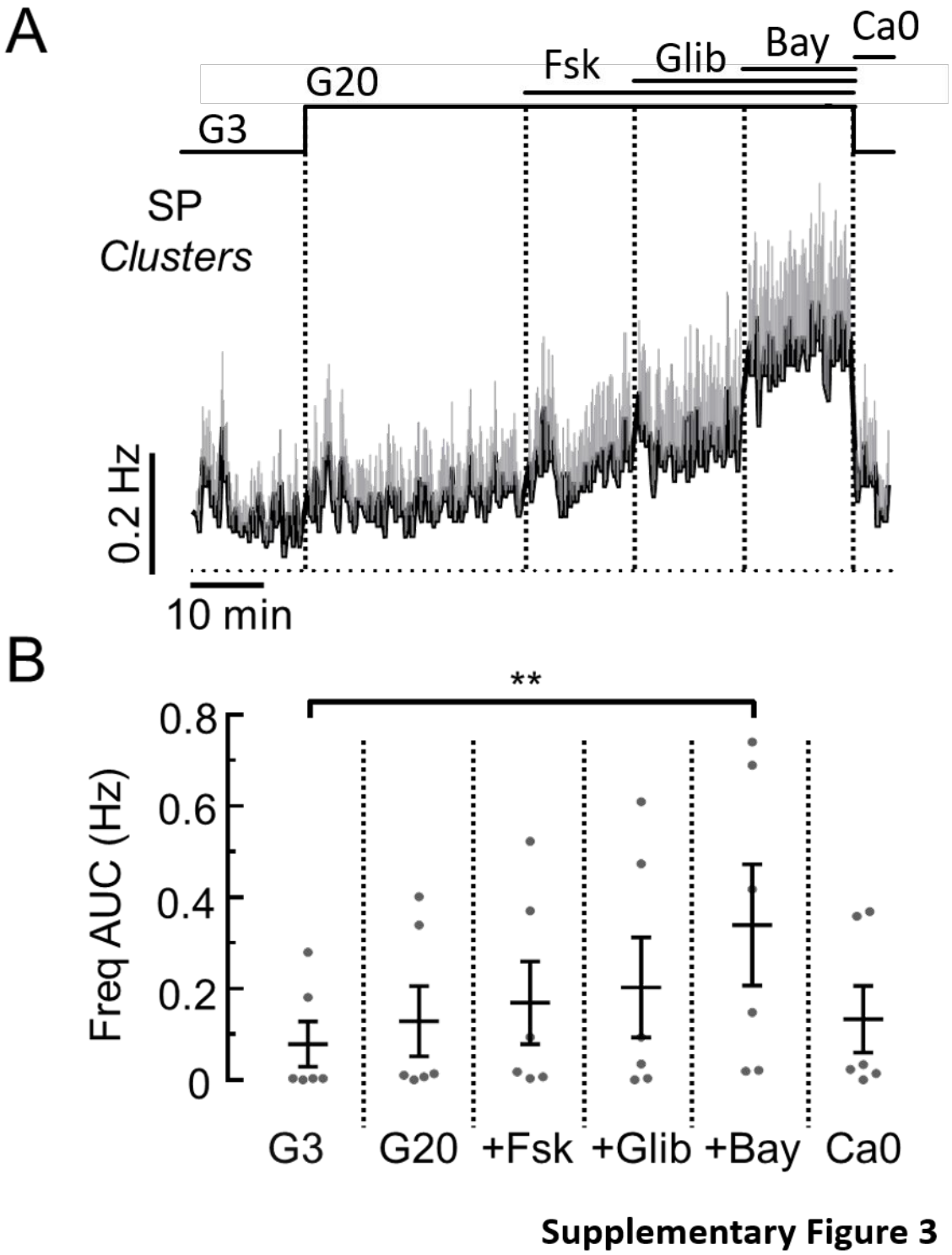

Supplementary Figure 3: Functional quality control with MEAs of a cluster preparation of BLCs. (**A**) Kinetics of SP frequencies (means +SEM) of BLCs in clusters in response to several stimuli: 3 mM glucose (G3), 20 mM glucose (G20) alone, followed by successive

additions of forskolin (Fsk, 1 μM), glibenclamide (Glib, 100 nM) and Bay K8644 (Bay, 10 μM). At the end of the protocol, G3 without calcium (Ca0) was applied to inhibit calcium entry (n=10). (**B**) Statistics on AUCs of SP frequencies (normalized over time) measured in (**A**) (n=10, **p<0.01; Friedman test).

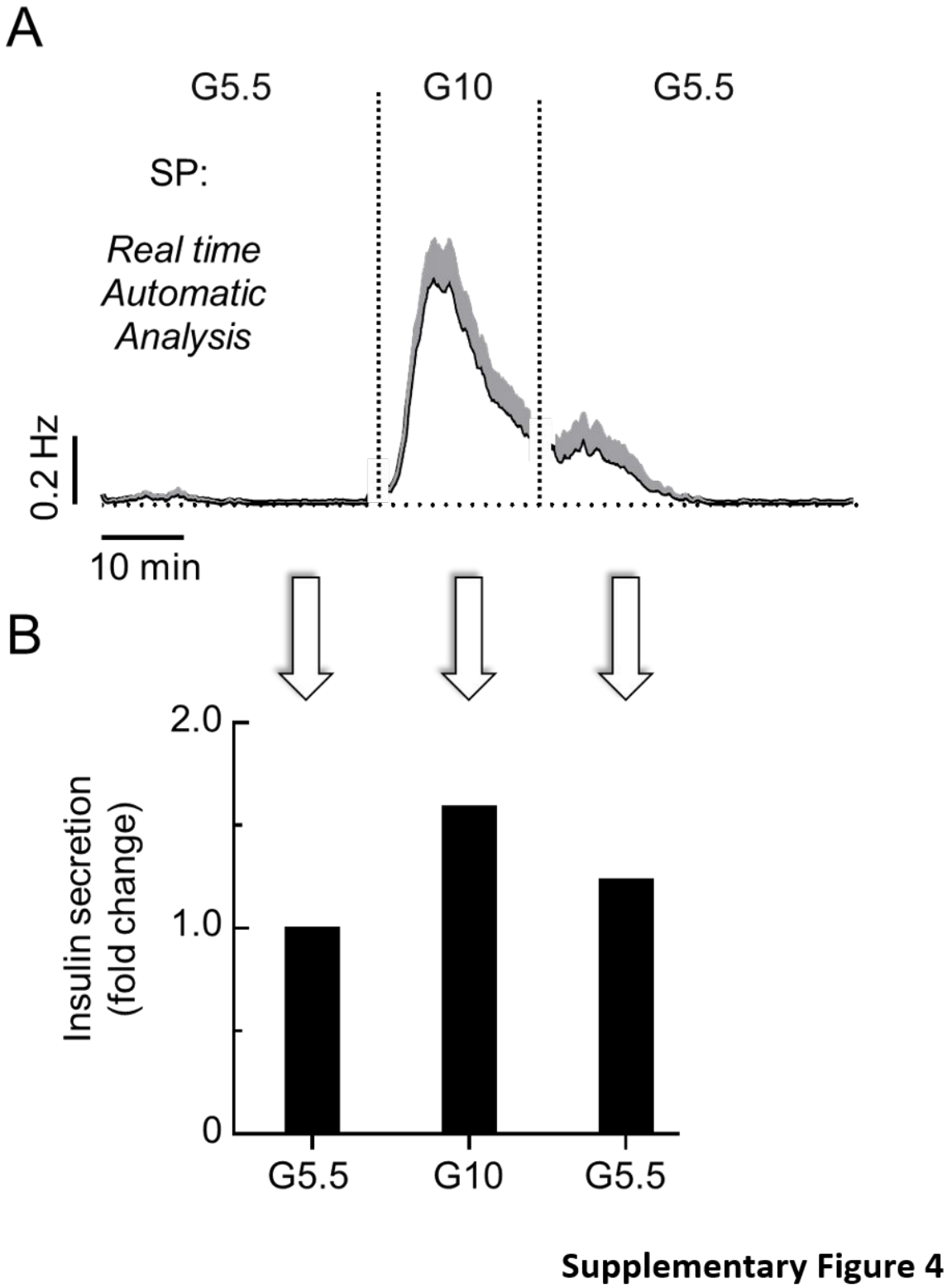

Supplementary Figure 4: Combination of automatic microelectronic analysis of SPs and insulin secretion. (**A**) Real time automatic hardware determination of SP frequencies (means

+SEM, n= 29) in BLCs in monolayer when glucose increases from 5.5 to 10 mM and then returns to 5.5 mM. (**B**) Corresponding insulin secretions (relative to the first G5.5).

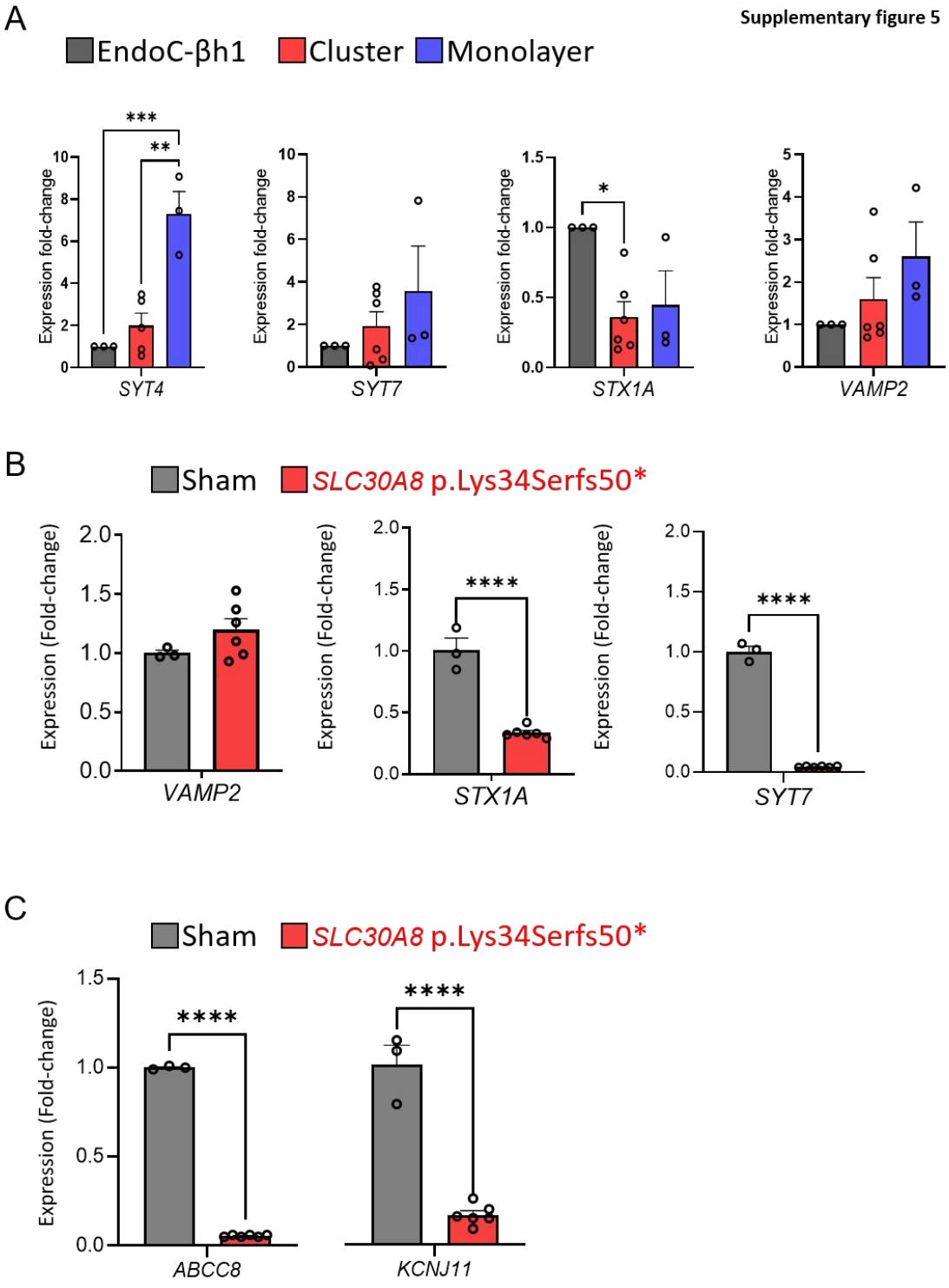

Supplementary Figure 5: Gene expression of key markers of secretory function in BLCs cluster and monolayer and in *SLC30A8*-edited clones. A. Expression of key genes

involved in exocytosis in EndoC-βH1 (n=3), BLCs in clusters (n=6) and monolayer (n=3). One-way ANOVA and Tukey. *p<0.05, **p<0.01, ***p<0.001. **B-C**. expressions of markers of exocytosis (B) as well as expression of K_{ATP} channel subunits *ABCC8* and *KCNJ11* (C) from one CRISPR-Sham clone (black) and two *SLC30A8*-edited clones (red) monolayer BLCs. Unpaired t-test, ****p<0.0001